AIChE WILEY InterScience DISCOVER SOMETHING GREAT

Scale-Up of a Continuous-Jet Hydrate Reactor for CO_2 Ocean Sequestration

Costas Tsouris, Scott McCallum, Douglas Aaron and David Riestenberg
Oak Ridge National Laboratory, Oak Ridge, TN 37831

Jorge Gabitto
Chemical Engineering Dept., Prairie View A and M University, Prairie View, TX 77446

Aaron Chow and Eric Adams
Dept. of Civil and Environmental Engineering, Massachusetts Institute of Technology, Cambridge, MA 02139

DOI 10.1002/aic.11117
Published online February 16, 2007 in Wiley InterScience (www.interscience.wiley.com).

In previous work in our laboratories and in the ocean, we have investigated the formation and dissociation of composite CO_2 particles made of CO_2 hydrate, liquid CO_2, and water. The composite is formed by partially converting liquid CO_2 into hydrate at mid-ocean depth (1000–1200 m) conditions. Partial conversion of CO_2 into hydrate enables injection of CO_2 in seawater in the form of a dense composite material that will drive CO_2 to ocean depths well below the injection point. Thermodynamic conditions allowing the formation of negatively buoyant composite particles have been established for a laboratory-scale, continuous-jet hydrate reactor (CJHR). An investigation has been performed to explore the issues related to the scale-up of the CJHR. Hydrate was formed using two CJHR geometries; the first sprayed water in CO_2, and the second sprayed CO_2 in water. Using a plot of Ohnesorge vs. Reynolds numbers allowed flow rates to be selected that would yield a spray regime and maximize hydrate formation. The effect of varying pressure and liquid flow rates on hydrate behavior was observed. Depending on these parameters, hydrate particles were observed to sink, float, or be neutrally buoyant. A two-order-of-magnitude scale-up in the flow rates of the two fluids has been achieved with the larger CJHR geometries without losing the important characteristics of the hydrate particles (i.e., density and cohesiveness). Temperature changes as a result of hydrate formation were also monitored. A mathematical model has been developed to predict the fate of sinking CO_2 hydrate particles after release in the seawater. These results can guide further field and laboratory investigations related to the scale-up of ocean CO_2 sequestration.
 AIChE J, 53: 1017–1027, 2007
Keywords: CO_2 sequestration, CO_2 ocean injection, CO_2 hydrate, hydrate reactor

Introduction

Atmospheric CO_2 currently has a concentration of ~375 ppm and is considered an important factor in global warming. It has been proposed that CO_2 levels reach no greater than 500 ppm atmospheric concentration, almost double the preindustrial concentration.[1] This goal has led to a considerable effort to efficiently separate and sequester anthropogenic CO_2.

Various technologies are being investigated for the separation of CO_2. In addition to the traditional technologies of absorption, adsorption, cryogenic distillation, and membrane diffusion,[2] novel methods are also being explored. Various

Correspondence concerning this article should be addressed to C. Tsouris at tsourisc@ornl.gov.

sequestration methods are also being investigated and include terrestrial, geologic, and oceanic options. Of these options, ocean sequestration is believed to have the highest storage capacity, limited mainly by potential marine environmental impacts. Barry et al.[3] estimate that up to 300 GtC could be stored in the deep ocean without decreasing the average pH by more than 0.18 units, comparable to levels of observed natural variability. There are currently few implemented sequestration projects, but considerable research is being performed to develop the technologies necessary to mitigate greenhouse gas buildup.

Pacala and Socolow conducted a review of greenhouse gas reduction technologies[1] that specifically detailed how various technologies could be combined to avoid the doubling of atmospheric CO_2 from the preindustrial era. They presented 15 technologies as a portfolio of energy options to mitigate greenhouse gas buildup over the next 50 years. These technologies could be mixed and matched, depending on local conditions, to achieve a stable atmospheric CO_2 concentration of about 500 ppm. This level would require the avoidance of ~175 GtC over a period of 50 years, which Pacala and Socolow divide into seven "wedges" of 25 GtC each. The ocean has the theoretical capability to fill this gap by itself and could clearly be a prominent player in combination with other technologies.

Direct ocean injection of CO_2

Ocean injection of anthropogenic CO_2 is under investigation as a possible method for preventing large amounts of CO_2 from entering the earth's atmosphere, thereby mitigating the greenhouse effect. Methods for ocean injection include injection as a buoyant liquid at depths between 800 and 1500 m to form a rising liquid droplet plume, injection as solid hydrate particles between 1000 and 2000 m to form a sinking particle plume, and injection below 3000 m to form a stable CO_2 lake on the ocean bottom.[4–6] Mid-depth (1000–2000 m) injection to form a sinking plume of particles containing liquid CO_2, water, and CO_2 hydrate is presented here, specifically regarding scale-up issues for ocean injection. Compared with droplet injection, this method is expected to drive CO_2 into the deep ocean for a more effective CO_2 sequestration in terms of residence time in the ocean. However, as with droplet injection, hydrate injection is still a dispersive method that is expected to cause lesser environmental effects than would the lake formation option.

Assuming that a typical coal power plant emits[3] 123 kg CO_2/s or about 1 Mt C/a, a Pacala-Socolow wedge would require the complete oceanic sequestration of the emissions of ~500 plants. This sequestration could be accomplished by injecting CO_2 at mid-depth points (~1000 m) to form sinking hydrate plumes to diffuse and dissociate well below the injection point.

CO_2 hydrate ocean injection

A small-scale (8.9-mm inside diameter [ID] outer tube) continuous-jet hydrate reactor (CJHR) (Figure 1) was developed at Oak Ridge National Laboratory (ORNL) to produce a sinking plume of CO_2 particles that will transport CO_2 to the deep ocean.[7,8] A composite of unreacted liquid CO_2, excess water, and hydrate produced by the CJHR will sink if >25% of the injected CO_2 is converted to hydrate at a depth of ~1000 m. This concept, as well as the relationship between the density of liquid CO_2, seawater, and hydrate composite at varying ocean depths, has been discussed by West et al.[8] CO_2 hydrate is a solid crystalline material with a chemical formula of $CO_2 \cdot n(H_2O)$, where n is the hydration number. Values of 6–8 have been reported for n[9]. The variability in the hydration number is a result of incomplete filling of the cavities formed by hydrogen bonding between water molecules. Using a CJHR, sufficient conversion could be achieved with suitable flow rates of water and CO_2 by having a high flow rate of water in the small, inner capillary (Figure 1) and a lower flow rate of CO_2 in the outer capillary. A sufficiently high flow of water establishes a spraying mode, which provides a high surface-area-to-volume ratio, aiding conversion of CO_2 to hydrate. Theoretically, for complete conversion of CO_2 into hydrate, a maximum volumetric flow-rate ratio of ~1:3 CO_2:H_2O is needed based on stoichiometry when n is assumed to take a value of 7.

It was observed by Tang et al.[10] and Riestenberg et al.[11] that three distinct breakup regimes form depending on the Ohnesorge and Reynolds numbers. Low Reynolds numbers result in the Rayleigh regime, in which uniform-size drops

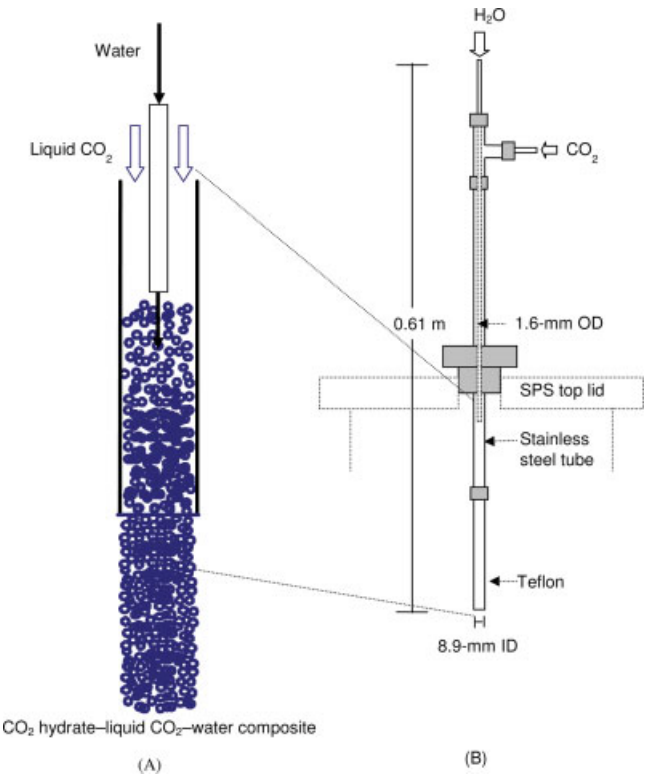

Figure 1. (a) CJHR receiving water (through the small capillary) and liquid CO_2 and producing a cohesive paste-like solid, which is a composite of CO_2 hydrate, unconverted liquid CO_2, and unconverted water; (b) CJHR mounted on the seafloor process simulator (SPS).

[Color figure can be viewed in the online issue, which is available at www.interscience.wiley.com.]

form from the destabilization of the jet. As the velocity is increased, transition breakup is observed. This mode is characterized by varying-size droplets formed by the jet destabilization. Spray mode is achieved at even higher Reynolds numbers. This mode has been deemed desirable because very fine droplets are formed, increasing the area for hydrate conversion. In the work of Riestenberg et al.,[11] various small capillaries were used with IDs ranging from 127 to 508 μm and outside diameters (ODs) ranging from 794 to 1588 μm. The flow rates in these experiments were constrained by the limits of the syringe pumps, but varied from 0.5 to 25.0 ml/min for both CO_2 and water. Increasing the injector throughput required a larger injector size. Riestenberg et al.[11] also measured the droplet-size distributions for different injectors and jet breakup modes. A significant observation was that the droplet size did not increase very much with capillary size when in spray mode (e.g., doubling capillary diameter produced a very small increase in drop size). The composite (liquid CO_2/CO_2 hydrate/water) material that forms in the spray regime is a cohesive paste-like solid with droplets fused by hydrate.[12] The composite has the same diameter as the internal diameter of the injector outlet and frequently breaks to form long, cylindrical particles of 50–100 mm length. A cohesive hydrate stream is desirable for aiding in transport of CO_2 to the deep ocean.

Investigations of sinking hydrate formation continued with field experiments at Monterey Bay in collaboration with the Monterey Bay Aquarium Research Institute.[7,13] Experiments using a larger injector (381 μm ID for water and 9.5 mm for CO_2) were performed at a depth of ~1200 m. Water and CO_2 flow rates were 140–150 ml/min and 26–40 ml/min, respectively. A remotely operated vehicle (ROV) was used to follow the movement of particles inside a "bubble box" and observe sinking/floating behavior. The bubble box was a large, transparent plastic box used to minimize the effect of ocean currents on the hydrate particles, thus producing a relatively quiescent bulk phase. The motion was, therefore, limited to the vertical direction and controlled by the buoyancy of the particles. The ROV was also equipped with instrumentation to record temperature, pressure, and seawater depth and salinity. The information recorded by the ROV allowed direct estimations of terminal velocity (~5 cm/s) and diameter shrinkage rates (4–10 μm/s) for the particles. Estimates of particle density were made from the terminal velocity by assuming a model for the drag coefficient of freely falling cylinders. The model, developed by Isaacs and Thodos,[14] had been observed to result in terminal velocities similar to those found using synthetic particles in our recent tank experiments.[13] Knowing the particle density as well as the densities of liquid CO_2, seawater, and hydrate allowed determination of the reaction efficiency X, which was calculated to be in the range of 30–50%.

This work focuses on scale-up issues of the CJHR with respect to CO_2 ocean injection. It is important that a spray regime is maintained to form cohesive and dense particles. As the cohesive composite sinks, it slowly dissolves into the seawater. This slow dissolution allows CO_2 to sink to greater depths. This paper describes the geometry and configuration for a two-order-of-magnitude scale-up of the CJHR. Characteristics of the composite product (e.g., density and cohesiveness) are discussed with respect to flow-rate increases associated with geometry changes of the CJHR. Scale-up of the CJHR required the addition of stronger pumps to the ORNL Seafloor Process Simulator (SPS) and construction of different injector geometries. Specific experiments discussed include determination of the inner capillary and outer tube diameters of the scaled-up CJHR by using water injected into cyclohexane. Cyclohexane was used because it mimics the behavior of CO_2 but can be examined at atmospheric conditions. Further experiments describe the geometry of two types of CJHRs, the first being a single-capillary concentric CJHR and the second being a capillary-array CJHR. Plume modeling to investigate the behavior of a sinking CO_2 hydrate composite plume is also described. Finally, a case study examines scale-up issues concerning the ocean sequestration of CO_2 from one full-sized power plant.

Experimental Methods

Experiments were performed in the ORNL SPS.[15] The SPS is a 72-l high-pressure (20 MPa) vessel made of Hastelloy C-22 metal with an internal diameter of 0.32 m and internal height of 0.91 m (Figure 2). The vessel is kept in a 2.5 m $\times$ 2.5 m $\times$ 2.1 m (height) refrigerated cold room equipped to maintain the desired experimental temperature. Sapphire viewing ports provide opportunities for visual observation, while various access ports allow for temperature and pressure instrumentation. The CJHR geometry in previous experiments included an inner tube of 1.6-mm OD and 127- to 508-μm ID and an outer tube of 9.5-mm OD and 6.4-mm ID. Water flow rates for these experiments were approximately 25 ml/min,

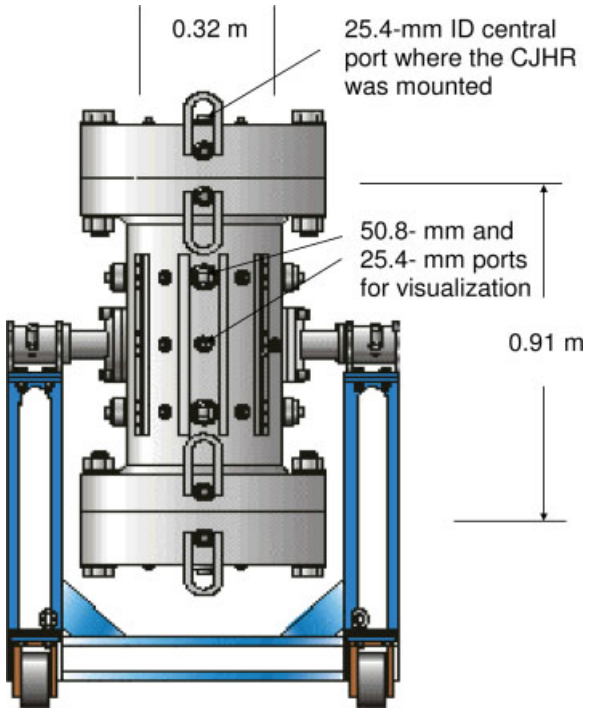

Figure 2. The ORNL SPS is a 72-l pressure vessel with multiple observation windows and various ports for instrumentation.

[Color figure can be viewed in the online issue, which is available at www.interscience.wiley.com.]

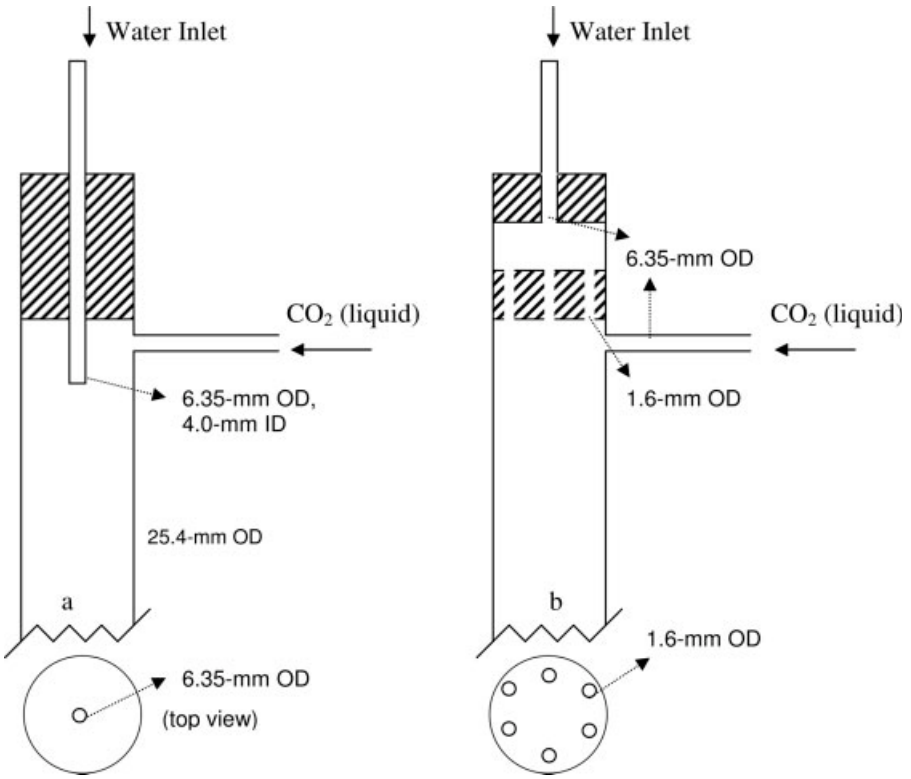

Figure 3. Two CJHRs used: (a) single-capillary, concentric injector and (b) capillary-array injector.

while CO_2 was injected at flow rates in the range of 5–10 ml/min. A sinking composite was achieved when the flow of water was approximately four times greater than the flow of CO_2. Hydrate-forming conditions for these experiments were in the proximity of 10 MPa and 4°C.[8,12]

A new, larger CJHR with a stainless steel, 4.0-mm ID and 6.35-mm OD inner tube and a Teflon® 25.4-mm OD outer tube has been constructed. The length of the reactor from the tip of the inner tube to the tip of the outer tube is ~0.61 m (Figure 3a). In addition to the single injector CJHR, a multiple co-flowing injector-array CJHR was designed with the objective of better distributing the dispersed phase in the continuous phase. The multiple injector array had six 1.6-mm ID channels (Figure 3b). These channels were evenly spaced about the circumference of the cross section of the outer tube. Both the single- and multiple-capillary CJHR used similar water and CO_2 flow rates for the sake of comparison.

The CJHR was mounted inside the SPS so that the entire reactor was submerged and at equilibrium with the vessel pressure. This arrangement allowed for the use of a submersible Seabird water pump (SBE 5T) that operated at high pressure and low head loss (Figure 4). The calibrated Seabird pump was situated inside the SPS, and it circulated water at a controlled flow rate through the CJHR, where it came into contact with liquid CO_2 injected from the outside of the SPS. This setup simulates injection of CO_2 in seawater.

The SPS was equipped with a pressure transducer, and thermocouples were installed at the CJHR outlet (5 mm from the tip of the reactor) and near the top of the bulk water volume. LabVIEW software was used to observe and record pressure and temperature conditions inside the SPS. Before injection experiments, the SPS was filled with ~60 l of water and allowed to cool overnight in the cold room to the experimental temperature. The experiments were started with an initial temperature and pressure of ~2.5°C and 11 MPa, respectively. Nitrogen gas was pumped through a Haskel booster pump (model No. 55790) to provide the necessary pressure in the SPS. A Haskel piston pump (Haskel ALG-60) was used to control the flow of CO_2 to the CJHR, while the Seabird submersible pump controlled the water flow. Because a large volume of CO_2 (660 ml/min) was added to the vessel, com-

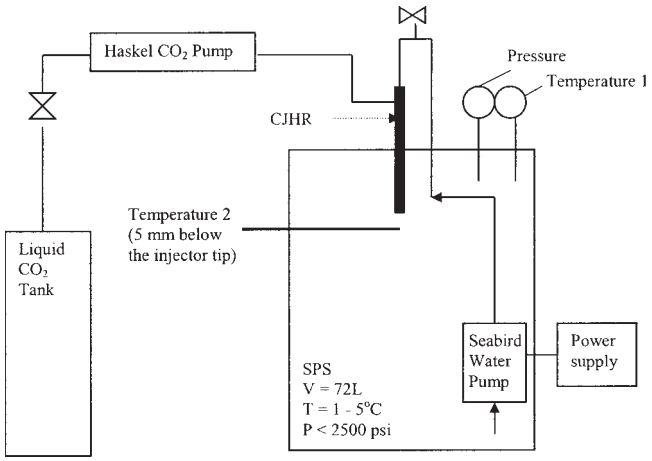

Figure 4. The experimental setup for the scale-up experiments included a submersible water pump operating at a high pressure and an externally mounted CO_2 pump.

pressed gas had to be manually vented periodically to maintain the desired pressure in the vessel. This pressure buildup and subsequent venting caused the pressure to vary between 11 and 11.7 MPa.

The scale-up experiments were video-recorded with a Sony™ FireWire (XCD-X710CR) camera connected to a personal computer and also observed with a Sony Handycam® (CCD-TR716). Fiber-optic lighting with focusing lenses provided light for the interior, while a white backdrop reduced glare from the metal walls. The 25.4-mm OD CJHR was placed vertically in the SPS and attached to the submersible water pump inside the vessel and to the CO_2 source through access ports on the side of the vessel. The injector was positioned such that the Sony camera could record the hydrate exiting the reactor.

Results and Discussion

Jet destabilization experiments have been conducted using capillary geometries similar to those of the scaled-up CJHR to obtain additional data on jet destabilization and spray formation relevant to this work. Cyclohexane was used as a substitute for liquid CO_2 at atmospheric temperature and pressure. The experimental arrangement described by Riestenberg et al.[11] has been employed for jet destabilization experiments. The difference here is that these experiments were conducted outside the SPS. A gear pump, delivering fluid through a flowmeter and a capillary, was used. Visual verification of jet breakup regimes and how they relate to injector diameter and injection flow rate were performed. Capillaries with diameters of 1-, 1.5-, 3-, and 4-mm ID were used at varying flow rates of water in cyclohexane. This series of experiments was performed to investigate whether the relationships introduced by Tang et al.[10] still apply at higher flow rates and injector diameters. The results are displayed with similar data from Tang et al.[10] and Riestenberg et al.[11] in Figure 5 in terms of the Reynolds number ($Re = \rho U d_o/\mu$) and Ohnesorge number $\lfloor Z = \mu(\rho\sigma d_o)^{-1/2} \rfloor$, where ρ, U, and μ are the density, velocity, and viscosity of the injected fluid, respectively; d_o is the capillary ID; and σ is the surface tension. It was determined by Tang et al., that a line of $Z = 18/Re$ is the boundary between transitional and spray regimes.[10] Points that appear to the right of this line in the Z vs. Re diagram will be in the spray regime. These data helped define the geometric dimensions of the scaled-up CJHR.

Using the scaled-up reactors shown in Figure 3, sinking hydrate composite was successfully formed in the SPS. Whereas previous total flow rates had been at most 200 ml/min in field experiments and 40 ml/min in the SPS, successful scale-up experiments were carried out with total flow rates exceeding 3000 ml/min. From visual observations of the hydrate composite particles flowing in the water column upon release in the SPS, it was determined that the capillary-array reactor shown schematically in Figure 3b formed more cohesive and denser composite particles than those formed by the single-capillary concentric reactor.

All but the most recent experiments using small and large reactors were conducted with water sprayed in liquid CO_2. This mode of operation was selected for two reasons: (1) for small reactors, where the flow rates are low, it makes sense to inject the fluid with the higher flow rate (in this case water) through the internal capillary to achieve better mixing conditions, and (2) when the inverse system (i.e., spraying CO_2 in water) was investigated, small capillaries were prone to clogging as a result of hydrate formation at the capillary tip. Both of these problems can be overcome when larger reactors are employed, which allow both modes of operation, as long as a spraying mode of jet breakup is achieved. Figure 6 shows a comparison of the hydrate formed from two different reactors and operating modes. Figures 6a,b show the hydrate composite formed using the capillary-array injector (Figure 3) when water is sprayed in liquid CO_2.

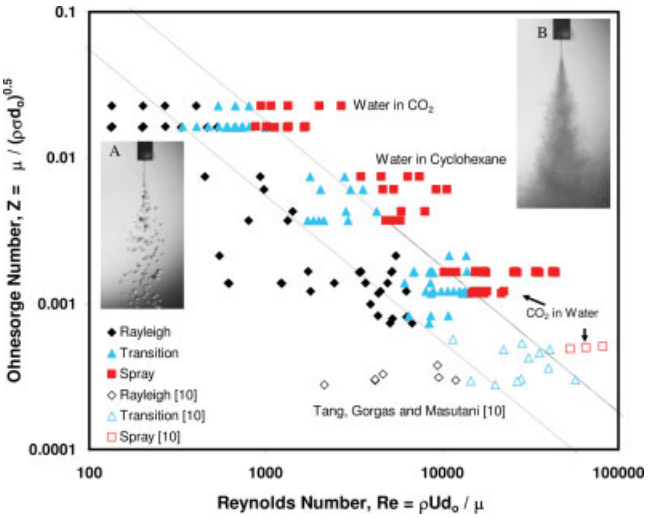

Figure 5. Jet breakup regimes identified in the Ohnesorge vs. Reynolds number diagram.

Data represented by solid symbols for "Water in CO_2" and "CO_2 in Water" were obtained by Riestenberg et al. in previous work.[11] Insets: Breakup regimes of water in liquid CO_2 in Rayleigh (a) and spray (b) modes. [Color figure can be viewed in the online issue, which is available at www.interscience.wiley.com.]

Figure 6b shows how a composite particle is formed when a stroke occurs in the CO_2 pump. The stroke duration of the pump was measured for three different pumping frequencies using an oscilloscope and was found to have an average duration of 135 ms (with a standard deviation of 18 ms). The fact that the stroke duration is independent of the pumping frequency shows that only the time between strokes is changing with frequency and that the flow rate during a stroke is constant. Each stroke injects 11 ml, so the highest frequency of 60 strokes/min produces a maximum flow rate of 660 ml/min. It was observed that the ends of the particles were not as cohesive as their middles. This difference could have been caused by the breakup of the particles at the exit of the injector at the end of each pump cycle. Each cycle delivered a sudden impact to the composite that caused this breakup. The incohesive ends of the hydrate composite particle are shown in Figures 6b,d. It should be noted here that cyclic pumps introduce the opportunity to control the length of the particles, as they exit the reactor, if the injected volume of the fluid per cycle can be adjusted.

Figure 6c shows composite formation using a single-capillary, concentric reactor with a capillary of 3.2-mm OD and 1.6-mm ID for liquid CO_2 sprayed into water. Breakup of the composite because of the pump stroke is shown in Figure 6d.

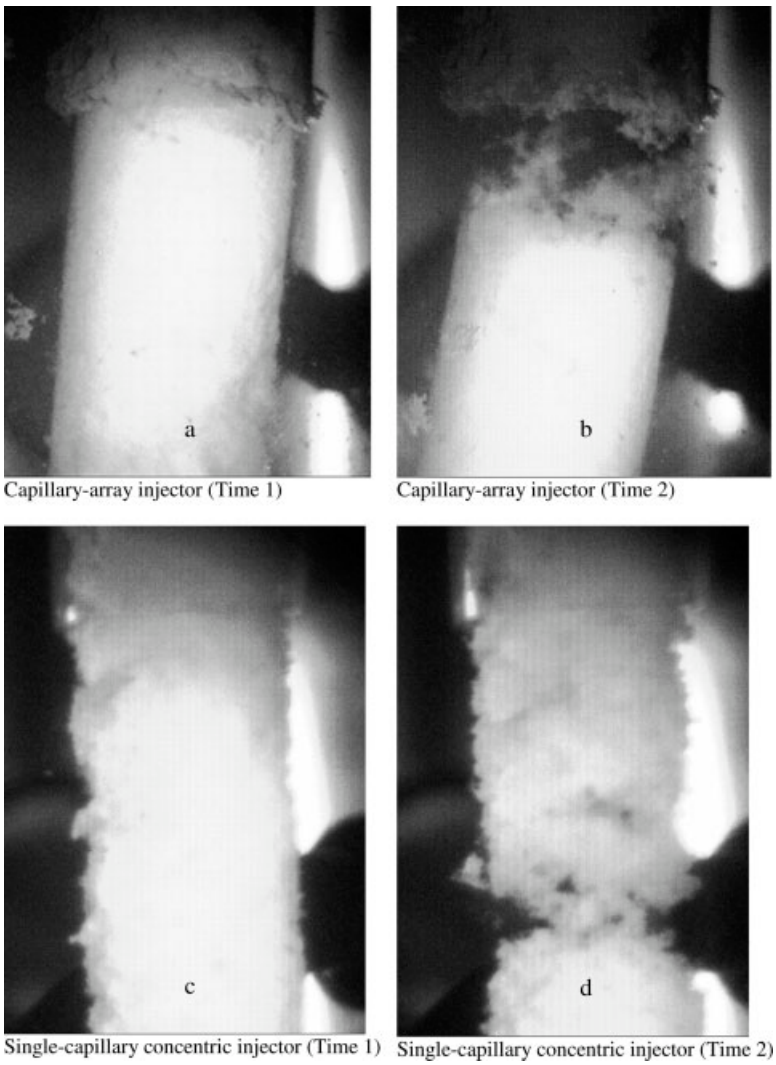

Figure 6. Comparison of particle formation under different spraying conditions: (a) water in CO_2, capillary-array CJHR; (b) water in CO_2, break in composite particle formed by a stroke in the CO_2 pump; (c) CO_2 in water, single capillary concentric injector; (d) CO_2 in water, break in the composite particle formed by a stroke in the CO_2 pump.

Some of the differences we visually observed for the two operating modes of the dispersion included (1) a smooth composite surface for the water-in-CO_2 system (Figures 6a,b) as opposed to the rough surface evident for the CO_2-in-water system (Figures 6c,d), (2) longer composite particles for the CO_2-in-water system and (3) denser composite particles for the CO_2-in-water system. We also observed that the surface of the CO_2-in-water composite became smoother, approaching that of the water-in-CO_2 composite, as the flow rate of water was decreased while the CO_2 flow rate was kept constant. It remains to be quantitatively proven with field experiments, but it seems that the CO_2-in-water spray produces denser composite particles in laboratory experiments with potentially greater sinking velocities, which is a desirable property with respect to sequestration efficiency. This behavior is probably caused by better spraying provided by the pulsed flow when liquid CO_2 (low-viscosity fluid) is sprayed into water (higher-viscosity fluid). Also, with the higher volume fraction of the continuous phase, the probability that the CO_2 droplets are surrounded by water is higher. Both of these facts lead to higher interphase mass transfer and conversion rates.

For the initial scale-up experiments, the SPS pressure was maintained at ~11 MPa, while the temperature was observed to rise steadily over the course of the experiment. Figure 7 shows the pressure and temperature data collected during the hydrate-formation experiment using the capillary-array injector. It can be seen that pressure spikes occurred during the experiment. These spikes were the result of pressure increases from CO_2 injection (the water was constantly recycled, and only CO_2 was added to the liquid volume) and pressure decreases from manually opening a vent valve to release gas to maintain pressure within a predefined range (11–11.7 MPa). The temperature at the injection point [5 mm from the end of the reactor (see Figure 4)] can be seen to rise

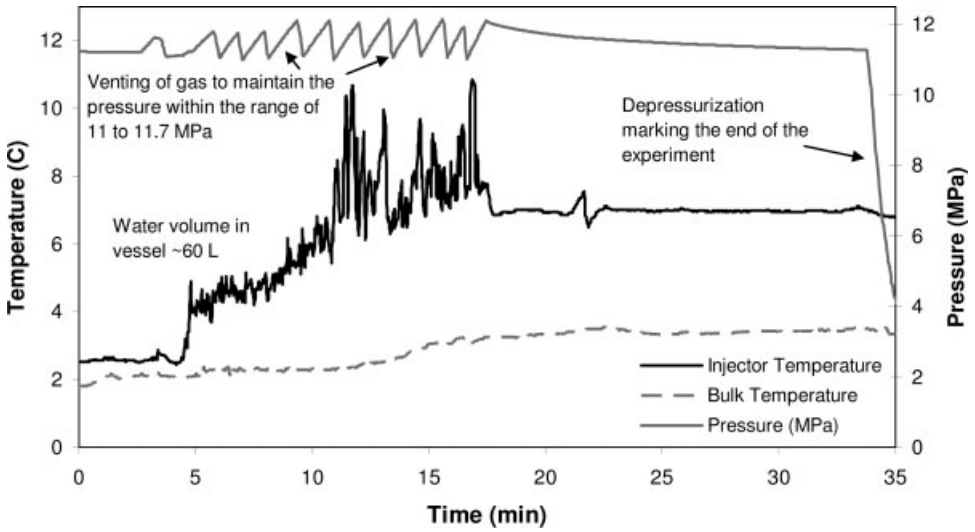

Figure 7. Temperature–pressure histories in SPS during an injection experiment with the scale-up CJHR.

sharply during injection as a result of the exothermic hydrate-formation reaction. The heat from this area was dispersed throughout the volume of the SPS, which led to the slow increase in temperature recorded in the bulk of the liquid. It is also evident that injection of liquid CO_2 stopped at ~18 min (Figure 7) because the pressure and injector temperature spikes ceased at that point. The vessel was allowed to equilibrate for another 17 min and then was depressurized.

A series of the CJHR scale-up experiments addressed hydrate formation at varying flow rates through the single-capillary CJHR. Water flow could be controlled by either manipulating the potential applied to the water-submersible pump or adjusting the external valve (shown in Figure 4) between the pump and the CJHR, while the CO_2 flow rate was controlled through the Haskel pump cycle frequency. Using higher water flow rates resulted in intense mixing in the reactor and a sinking hydrate composite was observed. Table 1 shows the conditions maintained in the SPS for cohesive hydrate production, while Table 2 shows the conditions for experiments in which the flow rates were varied at a constant pressure, as well as the behavior of the particles. From Table 2, sinking composite particles were produced only at high water flow rates (2600–3200 ml/min) and relatively high CO_2 flow rates (500–600 ml/min). At these flow rates, hydrate production was maximized, leading to denser composite particles. The excess water helped by (i) providing better mixing and (ii) reducing the temperature effects due to the exothermic reaction inside the reactor.

Table 1. Range of Operating Conditions Used in the Scale-Up Experiments

Pressure	(MPa)	10–13
Temperature	(°C)	1.5–3.7
H_2O Flow	(ml/min)	2000–3200
CO_2 Flow	(ml/min)	330–660
Injector ID	(mm)	1.6–4.0*

*ID was 4.0 mm for the single capillary and 1.6 mm for each of the six capillaries in the capillary-array injector.

Another series of scale-up experiments used the capillary-array CJHR with six channels of 1.6-mm ID to distribute the flow of water into smaller sprays. Sinking hydrate was formed in these experiments as well. Table 3 contains the pressure values, flow rates, and behavior of particles in these experiments. It can be seen that, at the lowest water flow rate (2400 ml/min), sinking particles were produced only at a relatively lower CO_2 flow rate and a relatively higher pressure (13 MPa). At higher water flow rates, sinking particles were produced at higher CO_2 flow rates and pressures ranging from 10.2–13 MPa.

It was also found that a cohesive, sinking composite could be formed if the combination of water flow rate and injector diameter corresponded to conditions to the right of the $Z = 32/Re$ line in Figure 5. This boundary was chosen from observations of the behavior of the composite particles rather than the jet break-up regime. It is above the $Z = 18/Re$ line reported by Tang et al.[10] and further from the transitional re-

Table 2. Experiments Conducted With the Single-Capillary, Concentric Injector

Q_{H_2O} (ml/min)	Q_{CO_2} (ml/min)	$\lambda(H_2O/CO_2)$	Behavior ( )
2000	330	6.06	Floating
2000	660	3.03	Floating
2200	330	6.67	Floating/NB
2200	440	5.00	Floating
2200	500	4.40	Floating
2200	660	3.33	Floating
2600	330	7.88	Floating
2600	500	5.20	Floating/NB
2600	660	3.94	Sinking/NB
2800	330	8.48	Floating
2800	500	5.60	Floating
2800	660	4.24	Sinking
3200	330	9.70	Floating/NB
3200	500	6.40	Sinking
3200	660	4.85	Floating

Temperature was 1.7–3.7°C.
Pressure was approximately 1600 psi.
NB denotes neutrally buoyant particles.

gime, and provides a more stringent criterion than the spray regime. As shown in Figure 8, the experimental conditions that produced sinking composite are located to the right of the boundary ($Z * Re \geq 32$). While hydrate could be formed for conditions found to the left of this line, sinking composite was observed when the flow rate of water was high enough to move the point to the right. For further experiments, the Weber number (We) provides a good summary of how the Re and Z numbers will predict the composite behavior. The relationship $We = (Re*Z)^2$ allows for a single number to predict whether a given diameter/flow-rate combination could yield a sinking, cohesive composite. Because sinking composite is formed when $Z * Re \geq 32$, if $We > 32^2$ (i.e., 1024), the hydrodynamic condition will be satisfied for a desirable product. This region results in a spray breakup pattern, however, it should be emphasized here that this condition is necessary but not sufficient for the formation of a sinking composite. There are also necessary thermodynamic and kinetic conditions that have to be satisfied, which are affected by pressure, temperature, length of the reactor, and flow rates of the reactants. Therefore, the We number criterion is necessary but not sufficient for the formation of sinking composite. For the experimental conditions of Tables 2 and 3, the We number was greater than 900.

During all series of experiments, hydrate was observed to accumulate at the bottom or top of the vessel after multiple tests. In some runs visual contact could not be maintained with the injector tip because abundant hydrate blocked the view. Hydrate was abundant because it formed faster than it dissociated, and it was stable because the water column of the vessel contained a high concentration of CO_2, which also affected the buoyancy of the particles. The higher the CO_2 concentration, the higher the water density is, and a higher particle density is needed for the particles to sink. In addition, the pressure was observed to drop slowly after injection ceased, indicating that some hydrate formation continued (e.g., liquid CO_2 was consumed, increasing the composite density) or that some CO_2 was continuing to dissolve into the water column. It should be noted here that the pressure drop was not due to leakage because the SPS was leak tested before and during each experiment.

Table 3. Experiments Conducted With the Capillary Array for Water Delivery in the Injector

P (MPa)	Q_{H_2O} (ml/min)	Q_{CO_2} (ml/min)	λ (H_2O/C_2O)	Behavior
13.0	2400	363	6.61	Sinking
13.0	2400	506	4.74	Floating
13.0	2400	429	5.59	Floating
11.6	2400	627	3.83	Floating
11.6	2400	396	6.06	Floating
11.6	2400	528	4.55	Floating
10.0	2400	528	4.55	Floating
10.0	2400	363	6.61	Floating
13.0	2700	660	4.09	Sinking
13.0	2700	539	5.01	Sinking
13.0	2700	660	4.09	Sinking
13.0	2550	660	3.86	NB
11.6	2700	594	4.55	NB
11.6	2700	506	5.34	Sinking
11.6	2700	429	6.29	Sinking
10.2	2700	682	3.96	Floating
10.2	2700	396	6.82	Floating
10.2	2700	594	4.55	Sinking

NB denotes neutrally buoyant particles.

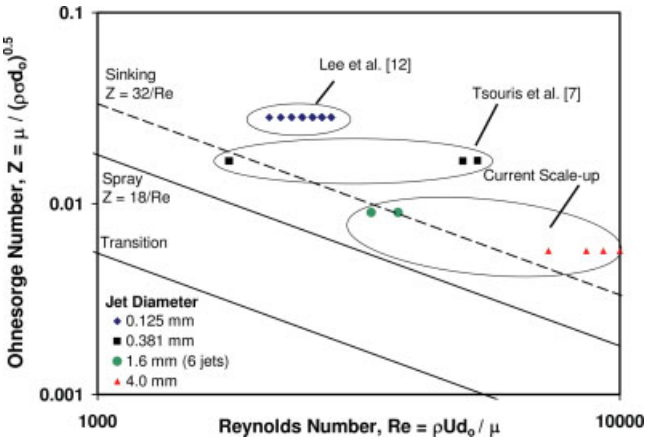

Figure 8. Ohnesorge vs. Reynolds number for hydrate composite formation using water/CO_2 co-flow injector of different geometries.

The $Z = 32/Re$ line indicates conditions that led to sinking hydrate. [Color figure can be viewed in the online issue, which is available at www.interscience.wiley.com.]

Calculated descent of composite particles

Because it is not practical in either the laboratory or the field to follow the entire descent of an individual particle, numerical calculations are made to predict the time-varying slip velocity $u_s(t)$ of representative particles as they shrink and descend through a typical ocean stratification off Keahole Point in Hawaii from Miller et al.[16] The slip velocity, u_s, is then integrated with time until the particle is completely dissolved to obtain a predicted sinking depth. The first set of columns of Table 4 shows the descent distance from the release depth of representative particles observed in the field by Riestenberg et al.[13] (typical length $l_p = 7$ cm, diameter $d_p = 0.7$ cm) for three values of hydrate conversion efficiency, X (0.3, 0.4, and 0.5), and three values of shrinkage rate (6, 8, and 10 μm/s). The predicted sinking distances of composite particles with a similar range of X and shrinkage rate, but with larger dimensions due to scale-up, are shown in the other columns of Table 4. The second column, "Laboratory_L05," reflects a typical particle observed in the present laboratory study, while the latter columns reflect additional factors of two in the scale-up of particle length (third column) and length plus diameter (fourth column).

The drag coefficient model of Isaacs and Thodos[14] for freely falling cylindrical particles is used to determine u_s. This model is applicable for values of Reynolds number based on d_p of $Re_d > 200$. As the composite particle shrinks with time, Re_d declines. When it drops significantly below 200, the model underestimates C_D, so Wadell's[17] model based on particle sphericity is employed, with the sphericity value chosen as 0.67 to match the predicted fall velocity for both models at $Re_d = 200$. For the particle described in column 1 of Table 4,

Table 4. Calculation of Descent Distance for Individual Particles and Particle Plumes With Different CO_2 Mass Loadings

Particle	Typical Field			Laboratory_L05			Laboratory_L10			Laboratory_fat_L10		
Length (cm)		7			5			10			10	
Diameter (cm)		0.7			2.54			2.54			5.08	
Shrinkage rate (μm/s)	6	8	10	6	8	10	6	8	10	6	8	10
$X = 0.30$; $\rho_p = 1047$ kg/m^3												
initial velocity (cm/s)		4.2			7.4			7.6			10.5	
Sinking distance of individual particle	34	26	21	206	155	124	217	164	131	567	432	349
Plume of CO_2 mass loading (kg/s):												
1	170	170	170	440	350	280	410	360	280	980	900	720
10	310	310	310	640	500	470	650	500	480	1260	1170	960
100	560	550	550	960	900	780	970	920	810	2020	1750	1350
1000	1120	1110	1100	2120	1120	1130	2190	1120	1140	3300	2440	2350
$X = 0.40$; $\rho_p = 1057$ kg/m^3												
initial velocity (cm/s)		5.6			9.9			10.2			14	
Sinking distance of individual particle	46	35	28	279	210	168	293	220	177	773	586	472
Plume of CO_2 mass loading (kg/s):												
1	170	170	170	490	360	330	530	360	350	1130	840	680
10	310	310	300	660	560	480	670	600	490	1480	1180	970
100	550	550	540	950	920	850	1170	940	870	2040	1810	1390
1000	1100	1090	1090	2210	1770	1090	2270	1870	1090	3300	2500	2430
$X = 0.50$; $\rho_p = 1068$ kg/m^3												
initial velocity (cm/s)		6.7			12.0			12.3			16.9	
Sinking distance of: individual particle	56	42	34	338	254	204	354	266	213	940	711	572
Plume of CO_2 mass loading (kg/s):												
1	170	170	170	530	430	350	550	440	360	1290	1000	810
10	300	300	300	780	620	480	820	640	490	1680	1230	1030
100	540	540	540	1260	930	870	1300	940	890	2510	1920	1390
1000	1080	1070	1070	2260	1920	1070	2340	2020	1070	3300	2470	2440

Densities (kg/m^3): Water: 1030, CO_2: 970, Hydrate: 1140.
Release depth = 1200 m, $V_{CO2}/V_W = 0.34$ within each particle.
Max. depth of density profile: 3300 m.

the Isaacs and Thodos model is applicable for the first 27% of the descent distance. However, because the initial values of Re_d are larger for the scaled-up particles (1300–6100), the Isaacs and Thodos model is applicable for a large proportion (89–96%) of the total descent depth for these particles (columns 2 through 4). For particles larger than those modeled, the Isaacs and Thodos model should be adequate for virtually the complete particle fall trajectory.

Table 4 shows how the individual-particle sinking distances vary with particle diameter, length, and conversion efficiency. It can be seen that the individual particle sinks significantly farther when the diameter is increased; smaller increases in individual particle sinking are achieved by decreasing shrinkage rate and increasing conversion efficiency for the same diameter. Only slight increases are achieved by increasing particle length because of the relatively weak dependence of u_s on the aspect ratio.

The particles are to ultimately be continuously released in large groups that form plumes. For each of the four particles modeled individually, therefore, analogous calculations are also made for steady particle plumes with various mass loadings (1, 10, 100, and 1000 kg/s of CO_2). The plume calculations are made using a modified version of the two-phase plume model by Wannamaker.[18] The model uses the same cylinder drag-coefficient model described above and takes into account the composition of the hydrate particle during dissolution. The model defines the final plume sinking distance (listed in Table 4) as the distance from the release depth at which 99% of the dispersed phase has completely dissolved. The calculated sinking distances significantly increase with increased mass loading as a result of the higher initial plume density, i.e., the total mass flux of particles and water divided by the plume volume flux at a given depth. As with individual particles, the plume sinking distance increases with increasing particle diameter because of the increased u_s, but the increase is not as great (e.g., for a plume with CO_2 mass loading of 1000 kg/s and conversion efficiency of $X = 0.4$, a change in diameter from $d_p = 0.7$ to $d_p = 5.08$ cm results in a two- to three-fold increase in sinking distance, while for individual particles, the sinking distance increases by a factor of about 17). Relatively modest increases in composite particle plume sinking are achieved by decreasing the particle shrinkage rate and increasing X, with the effect being more pronounced for larger diameters.

On the basis of the numerical results in Table 4, a motivation of scale-up methods of a particle release would proceed as follows, sorted by effect on resulting plume sinking: increase particle diameter, increase mass loading, increase conversion efficiency, decrease particle shrinkage, and finally, increase particle length.

Further scale-up of the CJHR

Formation of sinking CO_2 composite using a CJHR is possible when (1) the hydrodynamic, thermodynamic, and kinetic conditions are favorable and (2) the flow-rates of water and CO_2 are set at the appropriate levels. The *We* number should be greater than 1024, the temperature should be in the range of 0–5°C, and the pressure should be above 9.5 MPa. Although CO_2 hydrate forms at a lower pressure (~3.4 MPa

at 8.4°C), a higher pressure (>9.5 MPa) is needed to produce a sinking composite. The reason for this is that at a higher pressure, liquid CO_2 (which is compressible) becomes denser, adding to the density of the composite.

Observations suggest that it is reasonable to assume a flow rate of water at least four times larger than that of CO_2. For the scale-up of a single reactor, it is important to consider the flow rate of the composite and the spacing of the numerous adjacent reactors. Plume modeling can help to determine the scale-up design. For a single reactor, the mass flow rates of liquid CO_2 and water are defined. The option is then to operate the reactor in CO_2-in-water mode or water-in-CO_2 mode. To determine the preferred mode, field experiments for the CO_2-in-water spray mode will be compared with the composite density and dissolution rate of the water-in-CO_2 mode. After the mode is selected, the number of capillaries needed to distribute the dispersed fluid into the continuous phase will be determined. A higher conversion of liquid CO_2 into hydrate is aided by a good spatial distribution of the dispersed phase, while jet breakup occurs in the spray mode.

The recommended strategy is to assume a hexagonal configuration for the internal capillary array, with six capillaries located at the angles of a hexagon and at equal distance from the center and the internal surface of the outer tube. A seventh capillary will be located at the center of the hexagon. The diameters of all the capillaries will be the same. Using the known flow rate of the injected fluid through the capillaries (Q_d) and the Weber number criterion for a specific spray mode results in Eqs. 1 and 2 below:

$$We = (Re^* Z)^2 = \rho_d \, u^2 \, d_o/\sigma \geq 1024 \tag{1}$$

$$u = 4Q_d/(7\pi {d_o}^2) \text{(for seven capillaries)}, \tag{2}$$

where ρ_d is the density of the dispersed fluid. From these relationships, the capillary diameter for a spray mode is defined as shown in Eq. 3 below.

$$d_o \leq 0.032 \, (\rho_d {Q_d}^2/\sigma)^{1/3} \tag{3}$$

The internal diameter of the CJHR outlet tube can be determined as twice the distance between the center of the hexagonal capillary array and each of the angles. The length of the outer tube is such that the residence time of the fluid in the CJHR is ~5 s. By determining the configuration of the capillary array, the diameter of each capillary, the diameter of the outlet tube, and the length of the reactor, we have geometrically defined the CJHR for a given set of liquid CO_2 and water flow rates so that a sinking composite can be produced at intermediate ocean depths. This approach can be employed in scaling up the reactor for any set of flow rates.

Sequestration case study for one coal power plant

Preliminary estimations of what would be required for the sequestration of one coal power plant have been performed. Assuming the average power plant emits 123 kg CO_2/s (about 1 MtC/a), approximately 740 capillary-array CJHR units with 8.9-mm ID (for each of the seven capillaries) would be required for sequestration of all the CO_2 produced by that plant. This number is based on Eq. 3 for a continuous operation. The flow rate of CO_2 was determined using the CO_2 density at 1100 m depth and 4°C. Then, the flow of water was set to be four times that of CO_2 for optimum hydrate conversion.

Summary and Conclusions

We have developed and scaled-up a CJHR to convert liquid CO_2 and seawater to CO_2 hydrate and, thus, form a dense composite material at intermediate ocean depths. This material contains unconverted liquid CO_2, unconverted seawater, and hydrate and is expected to drive CO_2 well below the injection point for a more effective sequestration of CO_2 in the ocean. The reactor intimately combines liquid CO_2 with surrounding seawater in a mixing zone in which one phase is sprayed into the other. The drops of the sprayed phase fuse to each other by hydrate, generating a cohesive composite material that, depending on the conversion fraction of liquid CO_2 to hydrate, can be denser than the seawater and sink toward the bottom of the ocean.

Because of hydrate formation in the internal capillary of the reactor in the case of spraying liquid CO_2 into water in small CJHR geometries, this operation mode led to clogging problems and therefore was not successful. However, in the scaled-up reactor, where the ID of the capillary was significantly larger, both spraying modes were successful in producing composite particles denser than the surrounding seawater. In fact, based on visual observations, spraying CO_2 in water produced denser particles, which is believed to be the result of better spraying of the lower-viscosity fluid under a pulsed flow. This observation, as well as the dissolution rate of the particles, should be further investigated in field experiments.

On the basis of dimensionless analysis of the various jet destabilization regimes in the CJHR, a relationship has been derived (see Eq. 2) that relates the orifice-limiting diameter of the capillary to the physical properties and flow rates of the dispersed fluid so a dense composite can be produced. This relationship constitutes a necessary but not sufficient condition for the formation of sinking hydrate composite and can be used in scaling up the reactor. Additional thermodynamic and kinetic conditions are also necessary for sinking composite to be produced. Dissolution modeling described the history of particle diameter and terminal velocity and the depth of complete dissolution after injection.

A case study of ocean sequestration of CO_2 produced by a single power plant has also been discussed. An average plant producing 123 kg CO_2/s would require 740 CJHR units. Each unit would consist of a seven-capillary array, and each capillary would have an ID of 8.9 mm. This number of reactors would require additional work to determine the geometric configuration and spacing among the reactors based on plume modeling studies. Plume modeling also provides a clearer picture of the fate of composite particles as compared with modeling of individual particles. It is estimated that plume effects would allow particles to sink much deeper than individual particles before complete dissolution. As a recommendation for future work, field experiments are needed to further investigate the performance of an individual scaled-up reactor and observe the onset and the sinking behavior of plumes of composite particles produced by arrays of CJHRs.

Acknowledgments

Gratefully acknowledged is support by the Ocean Carbon Sequestration Program, Office of Biological and Environmental Research, U.S. Department of Energy under Contract No. DE-AC05-00OR22725 with UT-Battelle, LLC. The authors are thankful to Tommy Phelps and Phillip Szymcek for valuable discussions and Ms. P. P. Henson for editing the manuscript.

Literature Cited

1. Pacala S, Socolow R. Stabilization wedges: solving the climate problem for the next 50 years with current technologies. *Science*. 2004; 305:968–972.
2. Meisen A, Shuai X. Research and development issues in CO_2 capture. *Energy Convers Manage*. 1997;38(Suppl.):S37–S42.
3. Barry J, Adams E, Bleck R, Caldeira K, Carman K, Erickson D, Kennett J, McLain C, Sarmiento J, Tsouris C. Ecosystem and societal consequences of ocean versus atmospheric carbon storage. *Presentation to American Geophysical Union*, San Francisco, December 2005.
4. Medina M-G, Bond GM, Stringer J. An overview of carbon dioxide sequestration. The Electrochemical Society's *Interface*. 2001;10: 26–30.
5. Hoffert MI, Caldeira K, Benford G, Criswell DR, Green C, Herzog H, Jain AK, Kheshgi HS, Lackner KS, Lewis JS, Lightfoot HD, Manheimer W, Mankins JC, Mauel ME, Perkins LJ, Schlesinger ME, Volk T, Wigley TML. Advanced technology paths to global climate stability: Energy for a greenhouse planet. *Science*. 2002;298: 981–987.
6. Brewer PG, Friederich G, Peltzer ET, Orr FM Jr. Direct experiments on the ocean disposal of fossil fuel CO2. *Science*. 1999;284: 943–945.
7. Tsouris C, Brewer P, Peltzer E, Walz P, Riestenberg D, Liang L, West OR. Hydrate composite particles for ocean carbon sequestration: field verification. *Environ Sci Technol*. 2004;38:2470–2475.
8. West OR, Tsouris C, Lee S, McCallum S. Negatively buoyant CO_2-hydrate composite for ocean carbon sequestration. *AIChE J*. 2003; 49:283–285.
9. Holder GD, Gugini AV, Warzinski RP. Modeling Clathrate hydrate formation during carbon dioxide injection into the ocean. *Environ Sci Technol*. 1995;29:276.
10. Tang L, Gorgas TJ, Masutani SM. Liquid CO_2 Droplet Spectra. *In Proceedings of the Sixth International Conference on Greenhouse Gas Control Technologies*. Trondheim, Norway. 19–22 June, 2002.
11. Riestenberg D, Chiu E, Gborigi M, Liang L, West OR, Tsouris C. Investigation of jet breakup and droplet size distribution of liquid CO_2 and water systems-implications for CO_2 hydrate formation for ocean carbon sequestration. *Am Mineral*. 2004;89:1240–1246.
12. Lee S, Liang L, Riestenberg D, West OR, Tsouris C, Adams E. CO_2 hydrate composite for ocean carbon sequestration. *Environ Sci Technol*. 2003;37:3701–3708.
13. Riestenberg D, Tsouris C, Brewer PG, Peltzer E, Walz P, Chow A, Adams EE. Field studies on the formation of sinking CO_2 particles for ocean carbon sequestration: effects of injector geometry on particle density and dissolution rate and model simulation of plume behavior. *Environ Sci Technol*. 2005;39:7287–7293.
14. Isaacs JL, Thodos G. The free-settling of solid cylindrical particles in the turbulent regime. *Can J Chem Eng*. 1967;45:150–155.
15. Phelps TJ, Peters DJ, Marshall SL, West OL, Liang L, Blencoe JG, Alexiades V, Jacobs GK, Naney MT, Heck JL Jr. A new experimental facility for investigating the formation and properties of gas hydrates under simulated seafloor conditions. *Rev Sci Instrum*. 2001; 72:1514–1521.
16. Miller LA, Johnson WK, Arychuk M. Kona background survey, August 1999. *Chemical Data Report: Institute of Ocean Sciences, Canada*. 2000.
17. Wadell H. The coefficient of resistance as a function of Reynolds number for solids of various shapes. *J Franklin Inst*. 1934;217:459–490.
18. Wannamaker EJ, Adams EE. Modeling descending carbon dioxide injections in the ocean. *J Hydr Res*. 2006;44:324–337.

Manuscript received July 19, 2006, and revision received Dec. 12, 2006.